SUPERCONDUCTING QUADRUPOLE FOCUSING LENS

Part I: Analytical Design and Full-Scale Copper-Wound Pole

A. Asner
CERN
Geneva, Switzerland

I. INTRODUCTION

In 1966 CERN decided to design a first superconducting beam transport element, a quadrupole lens, with the aim of gaining operational experience with such magnets in external beams of the Proton Synchrotron and of sponsoring European superconductor technology.

A collaboration between CERN, the Culham Laboratory and the Oxford Instrument Company (both of the latter being in Great Britain) has since been established, the project being partially financed by the British Ministry of Technology.

This paper gives a theoretical analysis of the quadrupole lens and describes a full-scale, copper-wound pole model made at CERN with the aim of performing magnetic measurements and of establishing the winding procedure and the mechanical construction in view of the four poles to be wound with superconductors.

II. THE ANALYTICAL DESIGN OF THE QUADRUPOLE LENS

Several authors have considered the problem of obtaining accurate two-dimensional dipole, quadrupole — 2n pole fields in general — within a certain aperture by computing the required current density distribution around it. Grivet[1] has examined rectangular, uniform current density configurations; Beth[2] has developed a method of best approximation for an ideal sine-like line-current distribution around a circular aperture, since in any real case the current density and the coil height will be finite. The sine-like distribution is approximated by a number of uniform current density steps, yielding the required magnetic field, field gradient, etc. uniformity within the aperture.

The theory of the quadrupole lens under consideration is based on an independent though similar approach.[3-5] A finite current density and coil height around a circular aperture had been assumed and the appropriate configuration for uniform current density, yielding the (dipole) quadrupole field, etc., with required precision computed.

We start with the vector potential A at point P (ρ, ψ) of a line current $+I$ placed at r, φ, according to Fig. 1. Cylindrical coordinates are used.

---

1. A. Septier, European Organization for Nuclear Research Report CERN 60-6 (1960).
2. R.A. Beth, Brookhaven National Laboratory, Accelerator Dept. Report AADD-135 (1967).
3. A. Asner, F. Deutsch, and Ch. Iselin, CERN Report MPS/Int. MA 65-12, TN 75 (1965).
4. A. Asner and Ch. Iselin, in Proc. 2nd Intern. Conf. Magnet Technology, Oxford, 1967, p. 32.
5. F. Deutsch, CERN Report MPS/Int. MA 67-9, TN 90 (1967).

The vector potential at P is given by:

$$A = \tfrac{1}{2}\lambda \ln\left[r^2 + \rho^2 - 2r\rho\cos(\varphi-\psi)\right] \quad (1)$$

with

$$\lambda = \frac{I\mu_o}{2\pi} \quad . \quad (2)$$

The expression for the vector potential can be expressed as the following trigonometric power series[6]:

$$\frac{A}{\lambda} = -\tfrac{1}{2}\ln\left[r^2 + \rho^2 - 2r\rho\cos(\varphi-\psi)\right]$$

$$= -\ln r + \sum_{k=1}^{\infty} \frac{a^k \cos k(\varphi-\psi)}{k} \quad (3)$$

for $a = \rho/r < 1$, and as:

$$\frac{A}{\lambda} = -\ln\rho + \sum_{k=1}^{\infty} \frac{\cos k(\varphi-\psi)}{k\cdot a^k} \quad (4)$$

for $a = \rho/r > 1$.

For a symmetric arrangement of four line currents according to Fig. 2, the vector potential at $P(\rho,\psi)$ is:

$$\frac{A}{\lambda} = 4\sum_{k=1}^{\infty} \frac{a^{2k-1}}{2k-1}\sin\left[(2k-1)\varphi\right]\sin\left[(2k-1)\psi\right] \quad (5)$$

for $a = \rho/r < 1$.

If, according to Fig. 3, four symmetric sector coils with uniform current density j are assumed so that $dI = j\,r\,dr\,d\varphi$, and if the sectors cover the angular region between α and $(\pi/2)-\alpha$, etc., and between the radii R_1 and R_2 the vector potential A is given by:

$$A = 2\lambda\,(\sin 2\psi)(\cos 2\alpha)\,\rho^2 \ln\frac{R_2}{R_1} +$$

$$+\sum_{k=1}^{\infty} \frac{\sin\left[(4k+2)\psi\right]\cos\left[(4k+2)\alpha\right]}{2k(4k+2)^2}\,\rho^{4k+2}\left(\frac{1}{R_1^{4k}} - \frac{1}{R_2^{4k}}\right) \quad . \quad (6)$$

From the vector potential the magnetic field components B_ρ and B_ψ can be obtained as follows:

---

6. H.B. Dwight, Tables of Integrals and Other Mathematical Data (MacMillan, New York, 1955), Formula 418, p. 85.

$$B_\rho = [\nabla A]_\rho = \frac{1}{\rho}\frac{\partial A}{\partial \psi} = 4\lambda\ (\cos 2\psi)(\cos 2\alpha)\rho\ \ln\frac{R_2}{R_1} + \sum_{k=1}^{\infty} \frac{\cos[(4k+2)\psi]\cos[(4k+2)\alpha]}{2k(4k+2)}\rho^{4k+1}\left(\frac{1}{R_1^{4k}} - \frac{1}{R_2^{4k}}\right) \tag{7}$$

$$B_\psi = [\nabla A]_\psi = -\frac{\partial A}{\partial \rho} = -4\lambda\ (\sin 2\psi)(\cos 2\alpha)\rho\ \ln\frac{R_2}{R_1} - \sum_{k=1}^{\infty} \frac{\sin[(4k+2)\psi]\cos[(4k+2)\alpha]}{2k(4k+2)}\rho^{4k+1}\left(\frac{1}{R_1^{4k}} - \frac{1}{R_2^{4k}}\right)\ . \tag{8}$$

For $\psi = 0$, Eq. (7) yields the field B_ρ in the horizontal ρ-axis, and for $\psi = \pi/4$, Eq. (8) yields the field B_y or B_x, respectively. Differentiating Eqs. (7) and (8) under these conditions one obtains for the field gradient:

$$g_\rho = \left(\frac{\partial B_\rho}{\partial \rho}\right)_{\psi=0} = 4\lambda\ (\cos 2\alpha)\ \ln\frac{R_2}{R_1} + \sum_{k=1}^{\infty} 2\lambda\frac{(4k+1)}{k(4k+2)}\cos[(4k+2)\alpha]\ \rho^{4k}\left(\frac{1}{R_1^{4k}} - \frac{1}{R_2^{4k}}\right) \tag{9}$$

$$g_x = \left(\frac{\partial B_y}{\partial x}\right)_{\substack{\psi=45^\circ \\ x=\rho}} = 4\lambda\ (\cos 2\alpha)\ \ln\frac{R_2}{R_1} - 2\lambda\sum_{k=1}^{\infty} \frac{(-1)^k\cos[(4k+2)\alpha]}{k(4k+2)}(4k+1)\ \rho^{4k}\left(\frac{1}{R_1^{4k}} - \frac{1}{R_2^{4k}}\right)\ . \tag{10}$$

Equations (9) and (10) are very convenient for the design of a quadrupole lens: the first constant term corresponds to the wanted constant gradient, the sum to the error terms. By putting $\alpha = 15^\circ$, which in accordance with Fig. 3 corresponds to 30° sector coils, the first dodecapolar error term vanishes, and the gradient error is mainly determined by the 20th harmonic. A simple calculation shows that the same reasoning is valid for sector coils between the angles α_2 and $(\pi/4)(\alpha_2 - \alpha_1)$, respectively, between $(\pi/2) - \alpha_2$ and $(\pi/4) + (\alpha_2 - \alpha_1)$ (see Fig. 4).

Two ways of eliminating both the 12th and 20th harmonic and of obtaining an even more uniform gradient within the aperture are shown in Figs. 5 and 6. By introducing an intermediate sector radius R_i — as shown in Fig. 5 — and by introducing the angles α_1 and α_2 the g_ρ gradient (for example) becomes:

$$(g_\rho)_{\text{Fig. 6}} = 4\lambda \left(\cos 2\alpha_1 \ln \frac{R_2}{R_i} + \cos 2\alpha_2 \ln \frac{R_i}{R_1} \right) +$$

$$+ \sum_{k=1}^{\infty} 2\lambda \frac{(4k+1)}{k(4k+2)} \rho^{4k} \times \tag{11}$$

$$\times \left\{ \cos\left[(4k+2)\alpha_1\right] \left(\frac{1}{R_i^{4k}} - \frac{1}{R_2^{4k}} \right) + \cos\left[(4k+2)\alpha_2\right] \left(\frac{1}{R_1^{4k}} - \frac{1}{R_i^{4k}} \right) \right\} .$$

Choosing $\alpha_1 = 9^\circ$ and $\alpha_2 = 27^\circ$ the 20th harmonic is eliminated. The 12th harmonic is eliminated by choosing R_i such that

$$\cos 54^\circ \left(\frac{1}{R_i^4} - \frac{1}{R_2^4} \right) + \cos 162^\circ \left(\frac{1}{R_1^4} - \frac{1}{R_i^4} \right) = 0 \tag{12}$$

or

$$1.318 \frac{1}{R_i^4} = 0.88 \frac{1}{R_1^4} + 0.432 \frac{1}{R_2^4} = M ;$$

$$R_i = \sqrt[4]{\frac{1.318}{M}} . \tag{13}$$

If according to Fig. 6 two constant current density sectors with j_1 and j_2 are chosen, and again $\alpha_1 = 9^\circ$, $\alpha_2 = 27^\circ$, Eq. (9) changes into:

$$(g_\rho)_{\text{Fig. 7}} = 4\lambda_1 \cos 2\alpha_1 \ln \frac{R_2}{R_1} + 4(\lambda_2 - \lambda_1) \cos 2\alpha_2 \ln \frac{R_2}{R_1} +$$

$$+ \sum \frac{(4k+1)\ \rho^{4k}}{k(4k+2)} \left(\frac{1}{R_1^{4k}} - \frac{1}{R_2^{4k}} \right) \times$$

$$\times \left\{ 4\lambda_1 \cos\left[(4k+2)\alpha_1\right] + 4(\lambda_2 - \lambda_1) \cos\left[(4k+2)\alpha_2\right] \right\} . \tag{14}$$

The 20th harmonic is again eliminated with $\alpha_1 = 9^\circ$ and $\alpha_2 = 27^\circ$; the 12th harmonic by making:

$$4\lambda_1 \cos 54^\circ + 4(\lambda_2 - \lambda_1) \cos 162^\circ = 0 \tag{15}$$

$$j_2 = j_1 \frac{1.318}{0.88} = 1.5\ j_1 . \tag{16}$$

When designing superconducting quadrupoles it is important to know the field inside the winding in order to determine the mechanical forces and stresses as well as the magnetic field outside the winding.

By a similar computation as before one finds for the magnetic field components B_ρ and B_ψ inside the winding, i.e., for $R_1 < \rho < R_2$:

$$B_\rho = 4\lambda\,\rho(\cos 2\psi)(\cos 2\alpha)\,\ln\frac{R_2}{\rho} +$$

$$+\sum_{k=1}^{\infty}\frac{\cos[(4k+2)\psi]\cos[(4k+2)\alpha]}{2k(4k+2)}\,\rho\left[1-\left(\frac{\rho}{R_2}\right)^{4k}\right]+$$

$$+\sum_{k=1}^{\infty}\frac{\cos[(4k-2)\psi]\cos[(4k-2)\alpha]}{2k(4k-2)}\,\rho\left[1-\left(\frac{R_1}{\rho}\right)^{4k}\right] \tag{17}$$

$$B_\psi = -\,4\lambda\,(\sin 2\psi)(\cos 2\alpha)\,\rho\,\ln\frac{R_2}{\rho} -$$

$$-\sum_{k=1}^{\infty}\frac{\sin[(4k+2)\psi]\cos[(4k+2)\alpha]}{2k(4k+2)}\,\rho\left[1-\left(\frac{\rho}{R_2}\right)^{4k}\right]+$$

$$+\sum_{k=1}^{\infty}\frac{\sin[(4k-2)\psi]\cos[(4k-2)\alpha]}{2k(4k-2)}\,\rho\left[1-\left(\frac{R_1}{\rho}\right)^{4k}\right]\,. \tag{18}$$

For the field outside the quadrupole ($R_2 < \rho < \infty$) one finds:

$$B_\rho = 4\lambda\sum_{k=1}^{\infty}\frac{\cos[(4k-2)\psi]\cos[(4k-2)\alpha]}{2k(4k-2)}\,\frac{1}{\rho^{4k-1}}\left(R_2^{4k}-R_1^{4k}\right) \tag{19}$$

$$B_\psi = 4\lambda\sum_{k=1}^{\infty}\frac{\sin[(4k-2)\psi]\cos[(4k-2)\alpha]}{2k(4k-2)}\,\frac{1}{\rho^{4k-1}}\left(R_2^{4k}-R_1^{4k}\right)\,. \tag{20}$$

Similar expressions can be derived for dipole fields.[3-5] In order to obtain a field uniformity required for high energy physics beam transport and accelerator magnets, the elimination of a larger number of harmonics than in the quadrupole case will be necessary. When doing so, the method demonstrated approaches the analysis of Beth.

The CERN-Culham Laboratory quadrupole will be shielded by a magnetic steel cylinder, concentric with the longitudinal axis of the lens. It is useful to compute the minimum radius r_s of this cylinder as well as the effect of the imaged currents on the field and the field gradient within the useful aperture.

Normally one would choose $\rho = r_s$ such that the field components outside the quadrupole winding B_ρ and B_ψ [see Eqs. (19) and (20)] are B_ρ, $B_\psi \le B_{sat} \approx 2$ T.

The minimum cylinder thickness is found from Eq. (21):

$$\Delta_{min} = \frac{\Phi}{B_{sat}} \approx \frac{1}{B_{sat}}\int_{r_s}^{\infty}\lambda\cos 2\alpha\left(R_2^4 - R_1^4\right)\frac{d\rho}{\rho^3}$$

$$\approx \frac{1}{B_{sat}}\;\frac{\lambda\cos 2\alpha\,(R_2^4 - R_1^4)}{2\,r_s^2}\,. \tag{21}$$

In order to find the additional magnetic field $(B)_s$ or gradient $(g)_s$ due to the magnetic screen for a single sector, uniform current density quadrupole, the coordinate system shown in Fig. 7 will be used.

By imaging the winding radii on r_s one obtains:

$$R_1' = \frac{r_s^2}{R_1} , \quad R_2' = \frac{r_s^2}{R_2} \tag{22}$$

and for the imaged current density from:

$$j \; r \; dr \; d\varphi = j' \; r' \; dr' \; d\varphi' \tag{23}$$

$$j' = j \left(\frac{r_s}{r'} \right)^4 . \tag{24}$$

By a similar analysis as applied to the main winding field and gradient computation, one finds for:

$$\left(B_y\right)_{screen} = - \frac{\mu_o \; j \; r_s^4}{\pi} \sum_{n=0}^{\infty} \frac{4}{(4n + 2)(4n + 4)} \times$$

$$\times \; x^{(4n+1)} \sin \left[(4n + 2)\varphi_o\right] \left(\frac{1}{R_1'^{(4n+4)}} - \frac{1}{R_2'^{(4n+4)}} \right) \tag{25}$$

and

$$\left(g = \frac{\partial B_y}{\partial x} \right)_{screen} = - \frac{\mu_o \; j \; r_s^4}{\pi} \sum_{n=0}^{\infty} \frac{4 \; (4n + 1)}{(4n + 2)(4n + 4)} \times$$

$$\times \; x^{4n} \sin \left[(4n + 2)\varphi_o\right] \left(\frac{1}{R_1'^{(4n+4)}} - \frac{1}{R_2'^{(4n+4)}} \right) . \tag{26}$$

The gradient g according to Eqs. (9) and (10) is increased by

$$(\Delta g)_{screen} \approx \frac{\mu_o \; j}{2\pi} \sin 2\varphi_o \left[\left(\frac{R_2}{r_s} \right)^4 - \left(\frac{R_1}{r_s} \right)^4 \right] . \tag{27}$$

III. THE QUADRUPOLE PARAMETERS

Based on the expressions derived so far and taking into account the performance obtained with the NbTi composite superconductor wound test coil, as stated in paragraph 3 of the second part of this paper, written by D. Cornish, the nominal superconducting quadrupole parameters — without screening effect — have been chosen as follows (see Fig. 8):

Quadrupole length	l	70.0 cm
Winding inner radius	R_1	6.5 cm
Winding outer radius	R_2	14.8 cm
Useful aperture radius	R_o	5.0 cm
Screen radius	r_s	33.5 cm
Angles of sector coil	φ_1 ; φ_2	2^o; $(30-2)^o$
Over-all current density	j	1.15×10^4 A/cm
Nominal current	I	820.0 A
Nominal field gradient	g	57.0 Vs/m^3 (5.7 kG/cm)
Maximum field in winding straight part	$B_{o\ lin}$	4.5 T (45 kG)
Maximum end field	B_{max}	4.9 T
Maximum tangential and compressive winding stress	σ_t, σ_c	< 4.0 kg/mm^2
Quadrupole inductance	L	0.6 H
Stored energy	A	200 kJ

Figure 9 shows the quadrupole gradient errors on the main axes.

IV. WINDING OF A FULL-SCALE UPPER POLE

In order to gain experience in winding the four poles with a rather unusual geometry, a full-scale pole had been wound at CERN with a copper conductor of the final 1.52×4.05 mm^2 (0.06 in. $\times$ 0.16 in.) composite Cu-superconductor cross section.

Figure 10 shows the four pole cores and two of the 2^o side plates. Before winding, the core is clad with slotted, 1 mm thick vetronite (glass reinforced epoxy resin), providing electrical insulation and efficient helium flow into the winding.

Since the conductors are wound in layers parallel to the 28^o faces of the pole cores, the layers start to depart from the inner cylinder at point P (Fig. 8). As shown in Fig. 11 radial segments have been foreseen to guide the layers and determine the 90^o angle of a completely wound pole. In a similar way the upper circumferential segments determine the winding outer radius.

The model pole proved to be very useful in studying and determining many details of the winding technique such as twisting the conductor in order to obtain smooth layers in the coil straight parts, casting of the end helmet inner epoxy layers to fit closely the coil end geometry and machining of the 2^o side plates in strict accordance with the staircase-shaped straight coil parts.

The four coils will be slightly overwound so that when assembled with their side plates and pressed with the outer cylinder — one half of which is shown in Fig. 12 with helium passages and grooved vetronite insulation at the inside — a compact arrangement is obtained preventing relative displacements of individual conductors due to thermal and electromagnetic stresses.

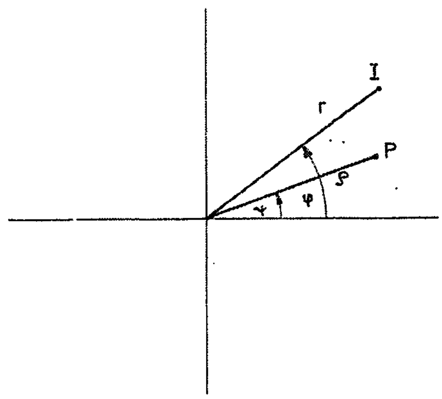

Fig. 1. Vector potential of line current $I(r,\varphi)$ in $P(\rho,\psi)$.

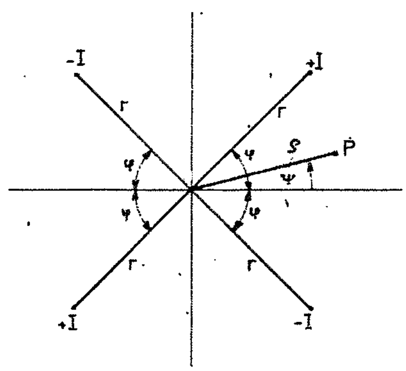

Fig. 2. Vector potential of four symmetric line currents $\pm$ I in $P(\rho,\psi)$.

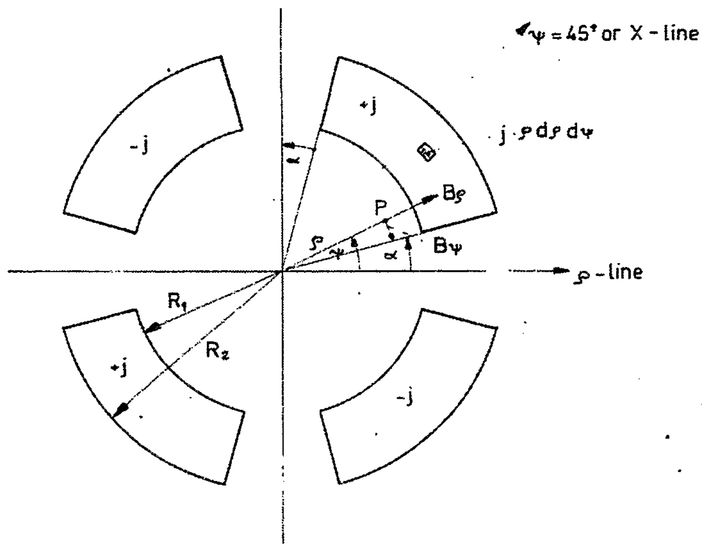

Fig. 3. Computation of field components B_ρ and B_ψ for constant current density - j (A/cm^2) - sector coils between the radii R_1 and R_2 and angles α and $(\pi/2) - \alpha$.

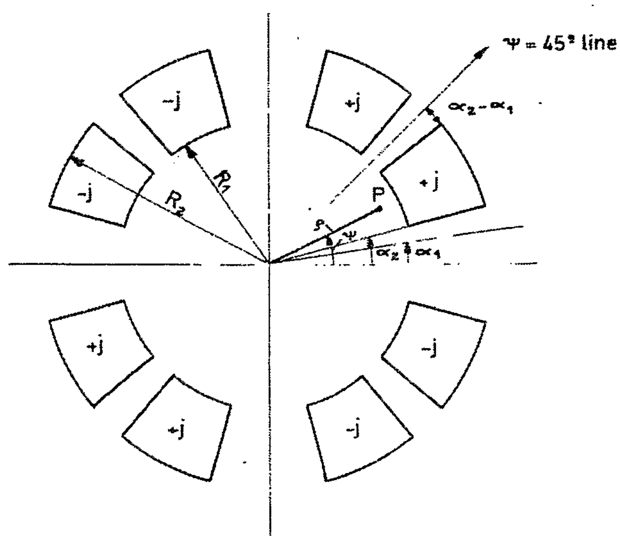

Fig. 4. Same, but for sector coils between $\alpha_2 - \alpha_1$ and $(\pi/4) - (\alpha_2 - \alpha_1)$.

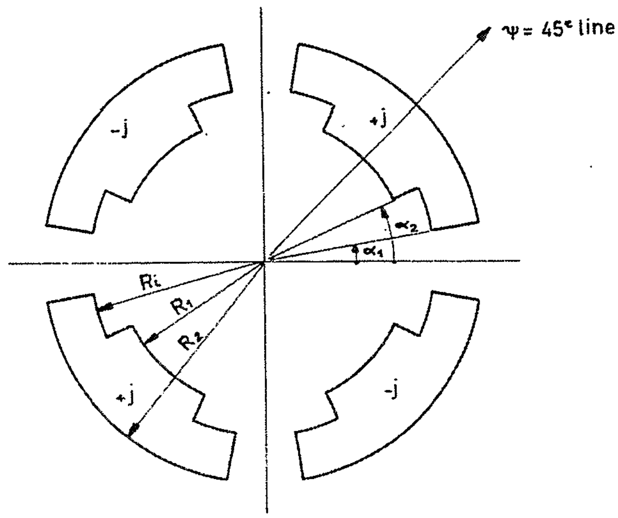

Fig. 5. Uniform current density sector coil quadrupole winding with intermediate radius R_1.

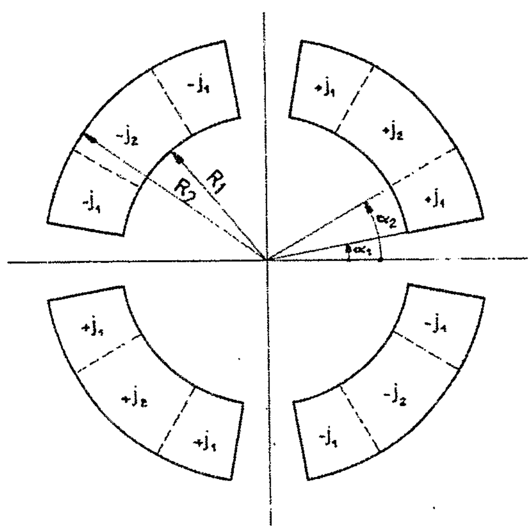

Fig. 6. Sector coil quadrupole winding with two current densities j_1 and j_2.

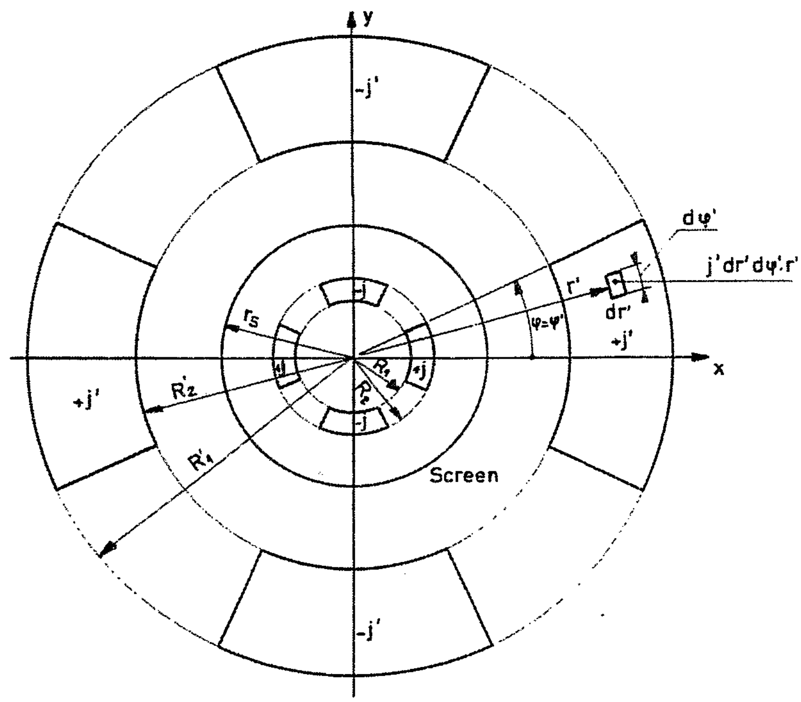

Fig. 7. Influence of concentric screen on uniform current density sector coil quadrupole winding.

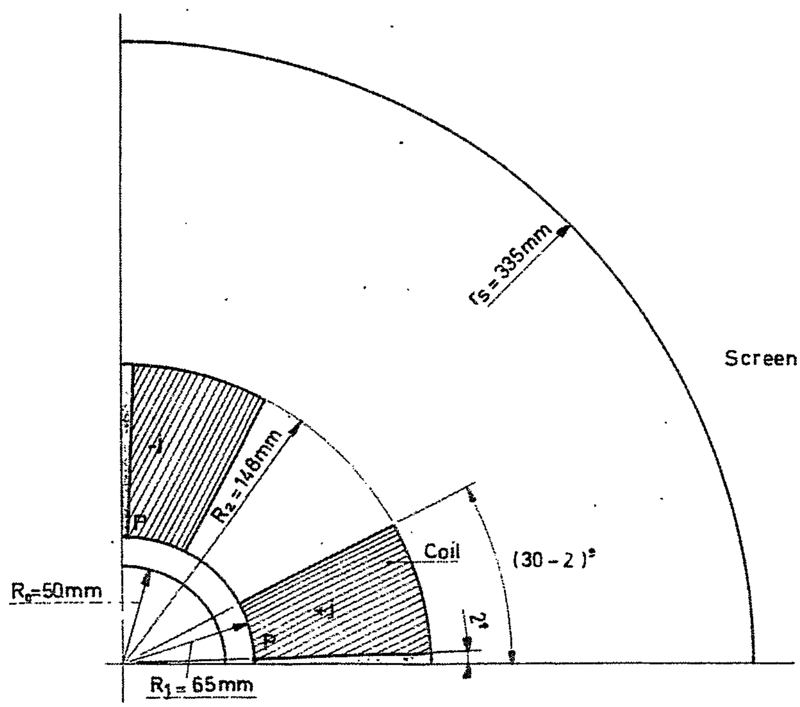

Fig. 8. Main geometrical parameters of the CERN superconducting quadrupole lens.

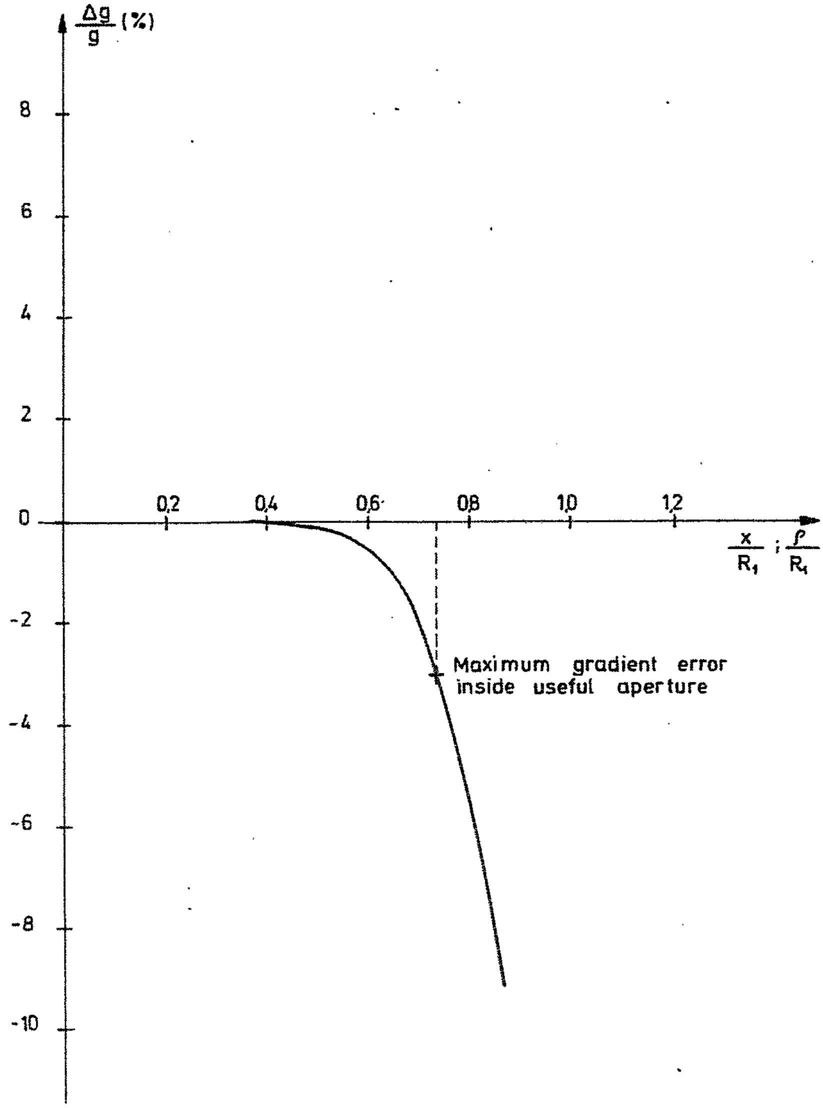

Fig. 9. Relative gradient error of the CERN SC quadrupole lens.

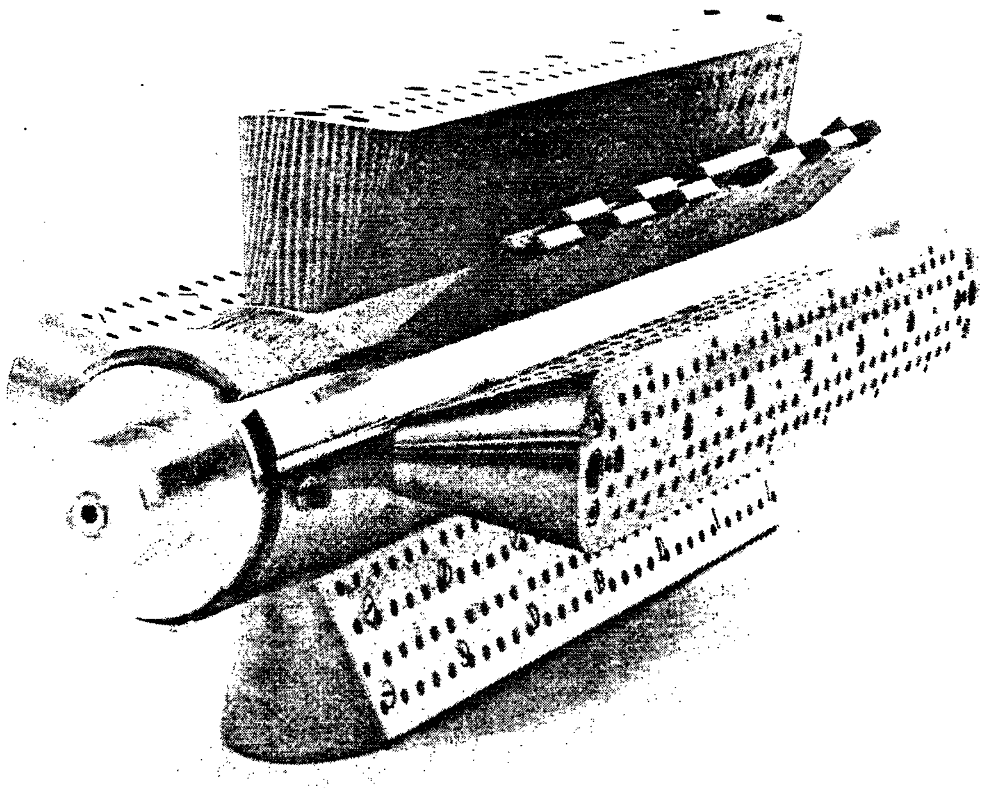

Fig. 10. The four pole cores, top one clad with vetronite, and two 2° side plates.

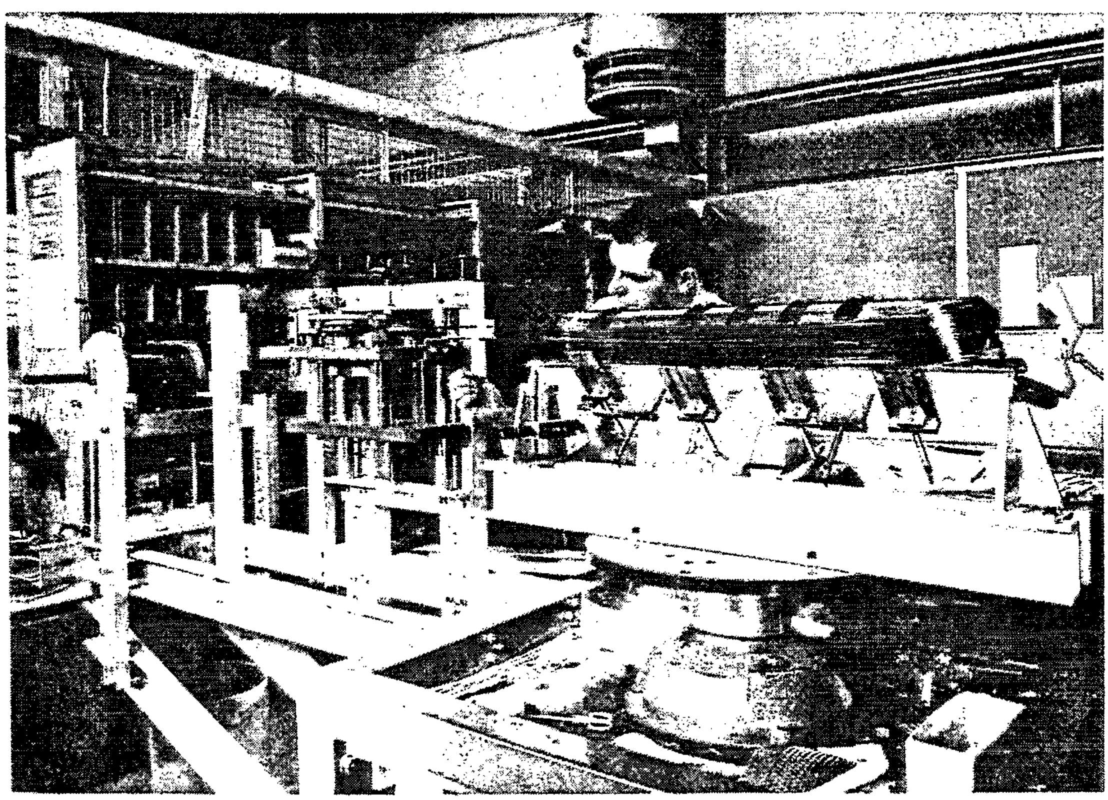

Fig. 11. Winding of the full-scale model pole with copper.

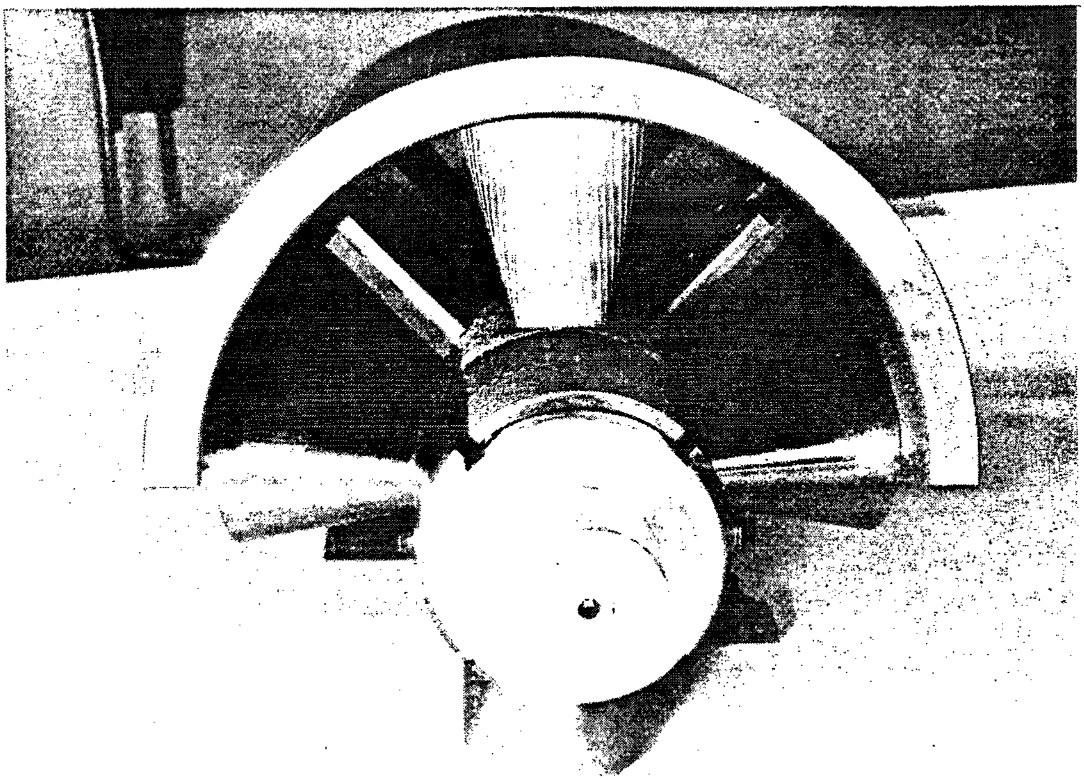

Fig. 12. Pole cores, 2° side plates and one-half of outside clamping cylinder.